

Fission fragment angular distribution in heavy-ion-induced fission with anomalous behavior

S. Soheyli* and B. Feizi

Bu-Ali Sina University, Department of Physics, Hamedan, Iran

(Received 8 June 2014; published 13 August 2014)

Fission fragment angular distribution in heavy-ion-induced fission reactions is of particular importance. Transition state theory is provided to determine the angular distribution of fission fragments which includes standard saddle-point statistical and standard scission-point statistical models. The standard saddle-point statistical model was not able to reproduce the experimental fission fragment angular anisotropies for several heavy-ion-induced fission systems. In contrast to the standard saddle-point model, the standard scission-point statistical model was fairly successful in the prediction of angular anisotropy in heavy-ion-induced fission reaction systems with an anomalous behavior in angular anisotropy of fission fragments, but this model is not widely used as the standard saddle-point statistical model. In this research, a generalized model is introduced for the prediction of fission fragments angular anisotropy in the heavy-ion-induced fission reaction systems having an anomalous behavior. For this purpose, we study the $^{14}\text{N}, ^{16}\text{O}, ^{19}\text{F} + ^{232}\text{Th}$; $^{16}\text{O}, ^{19}\text{F} + ^{238}\text{U}$; $^{24}\text{Mg}, ^{28}\text{Si}, ^{32}\text{S} + ^{208}\text{Pb}$; $^{32}\text{S} + ^{197}\text{Au}$; and $^{16}\text{O} + ^{248}\text{Cm}$ reaction systems. Finally, it is shown that the presented model is much more successful than previous models.

DOI: [10.1103/PhysRevC.90.024611](https://doi.org/10.1103/PhysRevC.90.024611)

PACS number(s): 25.70.Jj, 25.85.Ge

I. INTRODUCTION

The standard transition-state model was used to analyze fission fragment angular distributions. Usually two limiting assumptions on the position of the transition state and, correspondingly, two versions of the transition-state theory exist: the standard saddle-point statistical (SSPS) model [1], and the scission-point statistical (SPS) model [2]. Most of the information about the fission angular anisotropy is obtained within the framework of the SSPS model [3]. It is well known that the SSPS model reproduces reasonably well experimental data on the angular anisotropies of fission fragments for reactions induced by light projectiles like nucleons, ^3He , and alpha particles. Compound nuclei formed in these reactions have a temperature of about 1 MeV and low values of angular momentum [1,4]. In addition, experimental angular anisotropies show that the SSPS model in the prediction of the angular distribution of fission fragments from compound nuclei with high angular momentum, temperature, and fissility is unsuccessful [5,6]. For such systems, because of the presence of the noncompound nucleus fission events, fission fragment anisotropies have been observed to be anomalous in comparison to the prediction of the SSPS model.

The SPS model was proposed to predict the anomalous fission fragment angular distribution of such systems. The model assumes a well-defined configuration of scission point that the strong nonadiabatic effects retain statistical equilibrium, and then no nuclear interaction occurs between fragments [1]. In addition, it is assumed that the fission barrier was too small and the angular momentum and excitation energy of the compound nucleus are too large. This model is relatively accurate in the prediction of the angular distribution in fissions induced by projectiles around the oxygen [3].

The observation of anomalously large angular anisotropies in heavy-ion-induced fission reactions involving actinide targets resulted in a renewed interest in this topic [3,7,8]. The admixture of noncompound nucleus events such as quasifission, fast fission, and pre-equilibrium fission with the compound nuclear process was interpreted to be the possible reason for this anomalous behavior [9–18]. The average contributions of noncompound nucleus fission events are calculated for several heavy-ion-induced fission reactions having anomalous behaviors in fission fragment angular anisotropies [7]. It is also observed that the contribution of noncompound nucleus fission events increases with an increase in the mass number of projectile for a given target and this contribution exhibits a linear behavior as a function of the mass number of targets for a given projectile as well. The noncompound nucleus fission events involve full momentum transfer as in the case of compound nucleus fission events, but fission occurs before the formation of a fully equilibrated fissioning system. The signatures of noncompound nucleus fission events are broader or asymmetric mass distribution and higher anisotropy of the fission fragment angular distribution compared to that for compound nucleus fission.

An important issue is to provide a model that could be successful in the prediction of angular anisotropy for the systems with an anomalous behavior. Earlier calculations of fission fragment anisotropies within the framework of the SSPS model had been corrected to include the effects of pre-fission neutron emission, the alignment of ground-state nuclear spin with the nuclear deformation axis, and the effect of the relaxation time of K degrees of freedom on the variance of the K distribution [19–22].

In the present work, the upgraded saddle-point statistical (USPS) model is introduced in the prediction of angular anisotropy for the heavy-ion-induced fissions with an anomalous behavior.

To make the present paper self-contained, we study in Sec. II a brief description of the SSPS and the SPS models.

*s.soheyli@basu.ac.ir

Section III is devoted to introducing the USPS model. Section IV contains the calculations of angular anisotropies within the framework of the model. Section V is dedicated to a summary and conclusions.

II. STANDARD SADDLE-POINT AND SCISSION-POINT STATISTICAL MODELS

A. Standard saddle-point statistical model

According to the SSPS model, the symmetry axis at the saddle point could be known as the fission axis and direction of this axis does not change between the saddle and the scission points. In the framework of the SSPS model of the compound nucleus fission, the fission fragment angular distribution is determined by the total angular momentum I , its projection M on the space fixed axis, and its projection K on the body fixed symmetry axis that coincides with the direction of fission. The rotational energy $E_{\text{rot}}(I, K)$ of a nucleus with total angular momentum I and its projection K is given by

$$E_{\text{rot}}(I, K) = \frac{\hbar^2(I^2 - K^2)}{2\mathfrak{S}_{\perp}} + \frac{\hbar^2 K^2}{2\mathfrak{S}_{\parallel}}, \quad (1)$$

where \mathfrak{S}_{\perp} and \mathfrak{S}_{\parallel} are the moments of inertia perpendicular and parallel to the symmetry axis, respectively. Therefore, the rotational energy can be rewritten as

$$E_{\text{rot}}(I, K) = \frac{\hbar^2 I^2}{2\mathfrak{S}_{\perp}} + E_{\text{rot}}(K), \quad (2)$$

where $E_{\text{rot}}(K) = \frac{\hbar^2 K^2}{2} \left(\frac{1}{\mathfrak{S}_{\parallel}} - \frac{1}{\mathfrak{S}_{\perp}} \right) = \frac{\hbar^2 K^2}{2\mathfrak{S}_{\text{eff}}}$ is the change in rotational energy associated with $K \neq 0$ and the effective moment of inertia $\mathfrak{S}_{\text{eff}}$ is usually independent of K . It was shown these expressions, together with the dependence of the saddle-point level density on $E_{\text{rot}}(I, K)$, lead to a Gaussian distribution of K , centered around $K = 0$, which is characterized by the variance K_0^2 [23].

The variance of K distribution is given by

$$K_0^2 = \mathfrak{S}_{\text{eff}} T / \hbar^2, \quad (3)$$

where $T = \sqrt{\frac{E_{\text{ex}}}{a}}$ is the nuclear temperature of the compound nucleus at the saddle point. The quantity a is the level density parameter whose value is adopted from $A_{\text{C.N.}}/11$ to $A_{\text{C.N.}}/8$ ($A_{\text{C.N.}}$ is the mass number of the compound nucleus). The excitation energy of the compound nucleus at the saddle point (E_{ex}) is obtained from the following equation:

$$E_{\text{ex}} = E_{\text{c.m.}} + Q - B_f - E_{\text{rot}} - \nu_{\text{gs}} E_n, \quad (4)$$

In this equation, $E_{\text{c.m.}}$, Q , B_f , E_{rot} , ν_{gs} , and E_n represent the center-of-mass energy of the projectile, the Q value, the fission barrier height, the rotational energy of the compound nucleus, the number of pre-saddle neutrons, and the excitation energy lost from evaporation of one neutron from the compound nucleus prior to the system reaching the saddle point, respectively. In the calculation of E_{ex} , the pre-fission neutrons are usually taken to be emitted before the saddle point because it is not straightforward to separate experimentally the contribution of neutrons emitted before the saddle and the

ones emitted after the saddle but before the scission point. In this model, the fission fragment angular distribution $W(\theta)$ for the fission of spin zero nuclei is given by the following expression [1]:

$$W(\theta) \propto \sum_{I=0}^{\infty} (2I+1) T_I \times \frac{\sum_{K=-I}^I [(2I+1)/2] |D_{0,K}^I(\theta)|^2 \exp(-K^2/2K_0^2)}{\sum_{K=-I}^I \exp(-K^2/2K_0^2)}, \quad (5)$$

where T_I is the transmission coefficient for fission.

The angular anisotropy of fission fragments is defined as

$$A = \frac{W(0^\circ)}{W(90^\circ)}. \quad (6)$$

By the assumptions, $I + 0.5 \approx I$ and the I distribution is triangular, it can be shown that the fission fragment anisotropy is given by

$$A \approx 1 + \frac{\langle I^2 \rangle}{4K_0^2}, \quad (7)$$

where $\langle I^2 \rangle$ is the mean square angular momentum of the compound nucleus.

The prediction of angular anisotropy of fission fragments by using the SSPS model is valid only under restrictive assumptions. At high angular momentum, or at high fissility, the rotating liquid drop model (RLDM) predicts that the fission barrier height $[B_f(I)]$ vanishes even for a spherical nucleus, which leads to $K_0^2 \rightarrow \infty$. Subsequently, the distribution of K is uniform and hence the prediction of the SSPS model for the angular anisotropy of fission fragments is nearly uniform as shown by Eq. (7). This predicted tendency toward isotropy for fission fragments at high angular momentum is not seen in the experiments. This discrepancy is taken as a clear indication that the width of the K distribution is not determined at the predicted spherical saddle-point shape, but at a point where the nucleus is more deformed. Therefore, the SSPS model breaks down at high spin and/or large values of $\frac{Z^2}{A}$ of the compound nucleus, and the angular distribution of fission fragments is governed by an effective transition state different from the saddle-point transition state.

B. Scission-point statistical model

This model predicts angular anisotropies in reasonable agreement with those measured for heavy-ion-induced fission of some reactions where the fission barrier has vanished or become very small relative to the nuclear temperature. Although the formal equations for fragment angular distributions in the SSPS and SPS models are of the same structure, the variances in the distribution of angular momentum projections on the fission direction are established at very different stages of the fission process in the two models. The temperature of fission fragments at the scission point is defined as

$$T_{\text{sci}} = \sqrt{\frac{E_{\text{c.m.}} + Q_{\text{ff}} - E_k - E_{\text{def}} - E_{\text{rot}}(\ell) - E_{\text{ps}}}{2a}}, \quad (8)$$

where Q_{ff} , E_k , E_{def} , $E_{\text{rot}}(\ell)$, E_{ps} , and a are the Q value for the fission reaction, the total kinetic energy of fission fragments, the deformation energy of fission fragments, the orbital rotational energy for the angular momentum ℓ , the energy associated with pre-scission particle emission, and the level density parameter, respectively. The total excitation energy of the two fission fragments as a sum of their thermal and intrinsic rotational energies is given by $E - E_{\text{rot}}(\ell)$, where the orbital rotational energy for the angular momentum ℓ is

$$E_{\text{rot}}(\ell) = \frac{\ell^2 \hbar^2}{2\mu R_c^2}. \quad (9)$$

In this equation, μ is the reduced mass of the fission channel, and R_c is the distance between the centers of fission fragments at the scission configuration, assuming this configuration to be two spheres by the distance R_c that is given by the following equation:

$$R_c = 1.44 \frac{Z_1 Z_2}{E_k}, \quad (10)$$

where Z_1 , Z_2 are the atomic numbers of fission fragments, respectively [24]. The level density parameter in this model depends on the mass number of one of the symmetry fission fragments,

$$a = \frac{A_{ff}}{\lambda}, \quad (11)$$

where A_{ff} is the mass number of one of the symmetry fission fragments and λ is usually taken to be a number between 8 and 12. The variance S_0^2 for symmetric spherical fission fragments is given by the following equation [24]:

$$S_0^2 = \left(\frac{2\mathfrak{S}_0 T}{\hbar^2} \right) [(2\mathfrak{S}_0 + \mu R_c^2) / \mu R_c^2]. \quad (12)$$

The quantities \mathfrak{S}_0 and T are the moment of inertia and nuclear temperature of one of the symmetric fission fragments, respectively.

The variance S_0^2 for symmetric deformed fission fragments is also given by the following equation:

$$S_0^2 = \left(\frac{2\mathfrak{S}_{\parallel} T}{\hbar^2} \right) [(2\mathfrak{S}_{\perp} + \mu R_c^2) / (\mu R_c^2 + 2\mathfrak{S}_{\perp} - 2\mathfrak{S}_{\parallel})]. \quad (13)$$

Here, \mathfrak{S}_{\parallel} and \mathfrak{S}_{\perp} are the moments of inertia for a single fission fragment perpendicular and parallel to its symmetry axis at the scission point, respectively. The angular distribution of fission fragments within the framework of the SPS model for both spherical and ellipsoidal fission fragments and for a fixed excitation energy is given by the following equation [2,24]:

$$W(\theta) \propto \sum_{I_{\min}}^{I_{\max}} (2I+1) T_I \times \frac{\sum_{m=-I}^I [(2I+1)/2] |D_{M=0,m}(\theta)|^2 \exp(-m^2/2S_0^2)}{\sum_{m=-I}^I \exp(-m^2/2S_0^2)}, \quad (14)$$

a formula reminiscent of the corresponding formula [Eq. (5)] in the SSPS model. However, the variance K_0^2 is replaced by S_0^2 , and S_0^2 is calculated in a completely different way. The angular anisotropy in this model is also calculated by a similar equation as follows:

$$A \approx 1 + \frac{\langle I^2 \rangle}{4S_0^2}. \quad (15)$$

III. UPGRADED SADDLE-POINT STATISTICAL MODEL

It was known that the SSPS model leads to an underestimation of the measured fission fragment angular anisotropies in several heavy-ion-induced fission reactions. Because of the presence of the noncompound nucleus fission events, fission fragment anisotropies have been observed to be anomalous in comparison with the prediction of the SSPS model.

Back *et al.* have used an expression as a correcting factor which depends on the ratio of Coulomb to centrifugal energies to estimate the associated correction to the extracted values of K_0^2 as follows [17]:

$$K_0^2 = (\dot{K}_0)^2 \left[122 + \frac{I^2}{A^{\frac{4}{3}} Z^2} \right]^2. \quad (16)$$

They found an expression in terms of the fissility parameter χ and the y parameter of the rotating liquid drop model (RLDM) [25] by the following equation:

$$K_0^2 = (\dot{K}_0)^2 \left(1 + 1.245 \frac{y}{\chi} \right)^2, \quad (17)$$

where $(\dot{K}_0)^2$ is the standard deviation of the final (measured) total helicity distribution. The fissility parameter χ and the y parameter of the RLDM are given:

$$\chi = \frac{Z^2/A}{50.883 [1 - 1.7826 (\frac{N-Z}{A})^2]}, \quad (18)$$

$$y = \frac{1.9249}{[1 - 1.7826 (\frac{N-Z}{A})^2]} \frac{I^2}{A^{\frac{7}{3}}}. \quad (19)$$

By applying this correction and the assumption that the standard deviation of the K_0^2 distribution at the scission point is identical to the saddle-point K distribution, Back *et al.* obtained the following relation:

$$\left(\frac{\mathfrak{S}_{\text{sph}}}{\mathfrak{S}_{\text{eff}}} \right)_{\text{Back}} \approx \left(\frac{\mathfrak{S}_{\text{sph}}}{\mathfrak{S}_{\text{eff}}} \right)_{\text{RLDM}} \left(1 + 1.245 \frac{y}{\chi} \right)^{-2}, \quad (20)$$

where $\mathfrak{S}_{\text{sph}}$ is the rigid moment of a sphere of equal volume.

To upgrade the SSPS model, several factors can be corrected. In the present study, the effective moment of inertia of the compound nucleus at the saddle point is corrected, with the assumption that the calculated nuclear temperature, as well as the second moment of spin distribution of the compound nucleus based on the SSPS model at this point, are correct. For this purpose, the systematic study on the experimental data of fission fragment angular distribution for several heavy-ion-induced fission systems with an anomalous

TABLE I. The studied heavy-ion-induced fission systems along with their compound nucleus, Q values, and their fissility parameters.

Heavy-ion-induced fission system	Compound nucleus	Q value (MeV)	χ
$^{24}\text{Mg} + ^{208}\text{Pb}$	^{232}Pu	-74.05	0.800
$^{28}\text{Si} + ^{208}\text{Pb}$	^{236}Cm	-91.13	0.818
$^{32}\text{S} + ^{208}\text{Pb}$	^{240}Cf	-105.80	0.837
$^{14}\text{N} + ^{232}\text{Th}$	^{246}Bk	-25.62	0.817
$^{16}\text{O} + ^{232}\text{Th}$	^{248}Cf	-36.53	0.826
$^{19}\text{F} + ^{232}\text{Th}$	^{246}Es	-40.55	0.834
$^{16}\text{O} + ^{238}\text{U}$	^{254}Fm	-38.33	0.842
$^{19}\text{F} + ^{238}\text{U}$	^{257}Md	-43.17	0.849

behavior show that it is necessary to correct the above equation by using the rotating finite range model (RFRM) [26] for the calculation of effective moment of inertia and to introduce an adjustable parameter n^2 as shown by the following equation:

$$\left(\frac{\mathfrak{J}_{\text{eff}}}{\hbar^2}\right)_{\text{corr.}} \approx n^2 \left(\frac{\mathfrak{J}_{\text{eff}}}{\hbar^2}\right)_{\text{RFRM}} \left(1 + 1.245 \frac{y}{\chi}\right)^2. \quad (21)$$

It is also observed that the n can be parametrized in terms of the entrance channel mass asymmetry α [$\alpha = \frac{(A_T - A_p)}{(A_T + A_p)}$] (where A_T and A_p are the mass number of target and the mass number of projectile, respectively). The parameter $n(\alpha)$ is given by the following relation for the studied heavy-ion-induced reaction systems:

$$n(\alpha) = -14.08 + 36.34\alpha - 22.14\alpha^2. \quad (22)$$

IV. RESULTS AND DISCUSSION

In the present work, we determined the necessary quantities for the prediction of angular anisotropies within the SSPS, SPS, and the USPS models for eight heavy-ion-induced fission systems having an anomalous behavior in angular anisotropy. In Table I, the systems are listed along with their compound nucleus, Q values, and their fissility parameters χ .

Calculated necessary quantities for the prediction of angular anisotropies within the models are also given in Table II. The values of $\langle I^2 \rangle$ for the studied systems are taken from Refs. [17,22,27–31]. The level density parameter a is taken $\frac{A_{\text{C.N.}}}{8}$ ($A_{\text{C.N.}}$ is the mass number of the compound nucleus) for

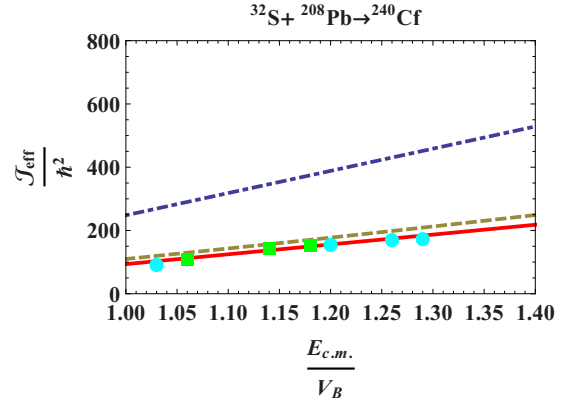


FIG. 1. (Color online) The effective moments of inertia at the saddle point for the $^{32}\text{S} + ^{208}\text{Pb}$ system. The continuous, dashed, and dot-dashed lines are the best fit on the experimental data, the calculated effective moments of inertia based on the USPS model, and the prediction of the RFRM, respectively. The experimental values of the effective moments of inertia denoted by circles and squares are taken from Refs. [17,27], respectively.

the angular anisotropies calculations based upon the SSPS and the USPS models. For the studied heavy-ion reaction systems, the derived effective moments of inertia at the saddle point based on the USPS model are in agreement with the experimental values of the effective moments of inertia as indicated for the $^{32}\text{S} + ^{208}\text{Pb}$ reaction system in Fig. 1. In this figure, the experimental values of the effective moments of inertia, the effective moments of inertia based on the RFRM, as well as the calculated effective moments of inertia for the $^{32}\text{S} + ^{208}\text{Pb}$ reaction system at the saddle point are shown. It can be clearly seen that for the system, the agreement between the calculated effective moments of inertia and the corresponding experimental data is satisfactory. The agreement between the experimental values of the effective moments of inertia and the calculated effective moments of inertia based on the USPS model are also observed for the other reaction systems. Figures 2–4 show the calculated angular anisotropies based upon the SSPS, the SPS, and the USPS models for the studied reaction systems. In these figures, points also show the experimental values of fission fragment angular anisotropies. It is observed that our results are in good

TABLE II. The studied systems and calculated necessary quantities for the prediction of angular anisotropies within the models.

Heavy-ion-induced fission system	Excitation energy (in MeV)	$(K_0^2)_{\text{SSPS}}$	$(\sigma^2)_{\text{SPS}}$	$(S_0^2)_{\text{SPS}}$	$(y(\langle I^2 \rangle))_{\text{USPS}}$
$^{24}\text{Mg} + ^{208}\text{Pb}$	32.63–61.15	$(143.29 + 0.030\langle I^2 \rangle)T_{\text{sad}}$	$39.59T_{\text{sci}}$	$93.06T_{\text{sci}}$	$6.27 \times 10^{-6}\langle I^2 \rangle$
$^{28}\text{Si} + ^{208}\text{Pb}$	31.72–58.84	$(136.99 + 0.036\langle I^2 \rangle)T_{\text{sad}}$	$40.73T_{\text{sci}}$	$95.60T_{\text{sci}}$	$5.98 \times 10^{-6}\langle I^2 \rangle$
$^{32}\text{S} + ^{208}\text{Pb}$	37.12–73.35	$(198.69 + 0.076\langle I^2 \rangle)T_{\text{sad}}$	$41.89T_{\text{sci}}$	$98.20T_{\text{sci}}$	$5.71 \times 10^{-6}\langle I^2 \rangle$
$^{14}\text{N} + ^{232}\text{Th}$	42.07–73.76	$(148.69 + 0.020\langle I^2 \rangle)T_{\text{sad}}$	$43.56T_{\text{sci}}$	$102.43T_{\text{sci}}$	$5.51 \times 10^{-6}\langle I^2 \rangle$
$^{16}\text{O} + ^{232}\text{Th}$	37.80–69.09	$(195.58 + 0.050\langle I^2 \rangle)T_{\text{sad}}$	$44.24T_{\text{sci}}$	$103.75T_{\text{sci}}$	$5.41 \times 10^{-6}\langle I^2 \rangle$
$^{19}\text{F} + ^{232}\text{Th}$	29.75–47.95	$(211.53 + 0.067\langle I^2 \rangle)T_{\text{sad}}$	$45.14T_{\text{sci}}$	$105.80T_{\text{sci}}$	$5.26 \times 10^{-6}\langle I^2 \rangle$
$^{16}\text{O} + ^{238}\text{U}$	26.76–96.54	$(200.00 + 0.140\langle I^2 \rangle)T_{\text{sad}}$	$46.04T_{\text{sci}}$	$107.85T_{\text{sci}}$	$4.97 \times 10^{-6}\langle I^2 \rangle$
$^{19}\text{F} + ^{238}\text{U}$	46.09–58.09	$(174.00 + 0.310\langle I^2 \rangle)T_{\text{sad}}$	$46.95T_{\text{sci}}$	$109.94T_{\text{sci}}$	$5.11 \times 10^{-6}\langle I^2 \rangle$

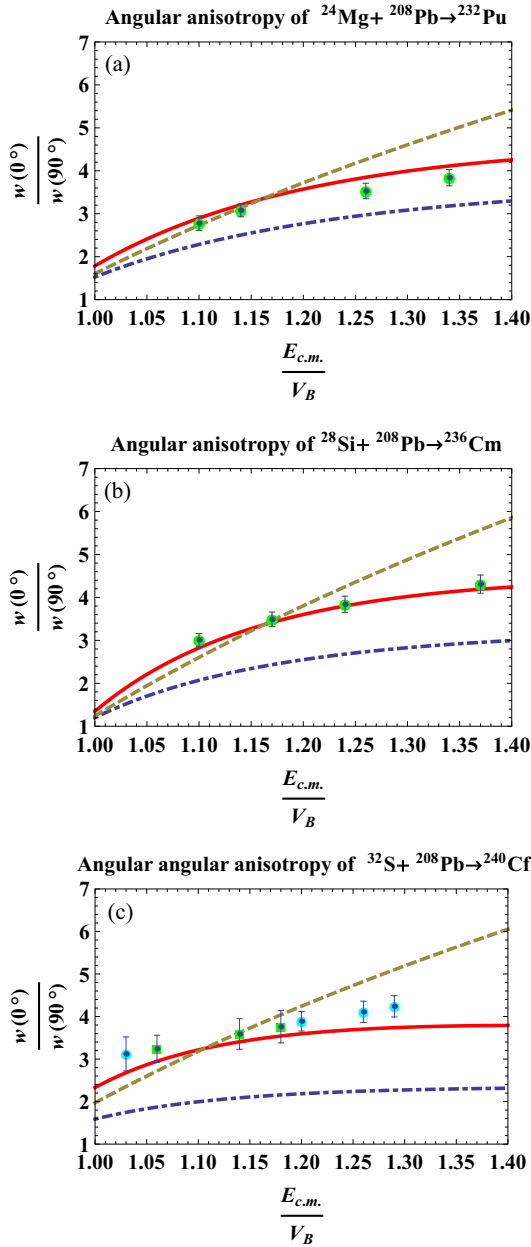


FIG. 2. (Color online) Experimental fission fragment angular distributions for the induced fission of the ^{208}Pb by different projectiles are compared with the predictions of the SSPS (dot-dashed curve), the SPS (dashed curve), and the USPS (continuous curve). (a) For the induced fission of the ^{208}Pb target by ^{24}Mg , the experimental values of angular anisotropy are taken from Ref. [17]. (b) For the induced fission of the ^{208}Pb target by ^{28}Si , the experimental values of angular anisotropy are taken from Ref. [17]. (c) For the induced fission of the ^{208}Pb by ^{32}S , the experimental values of angular anisotropy denoted by circle and square points are taken from Refs. [17,27], respectively.

agreement with the experimental data of angular anisotropies as shown in these figures.

It is well known that the entrance channel mass asymmetry parameter α with respect to the Businaro-Gallone critical mass asymmetry parameter α_{BG} plays a very dominant role in the

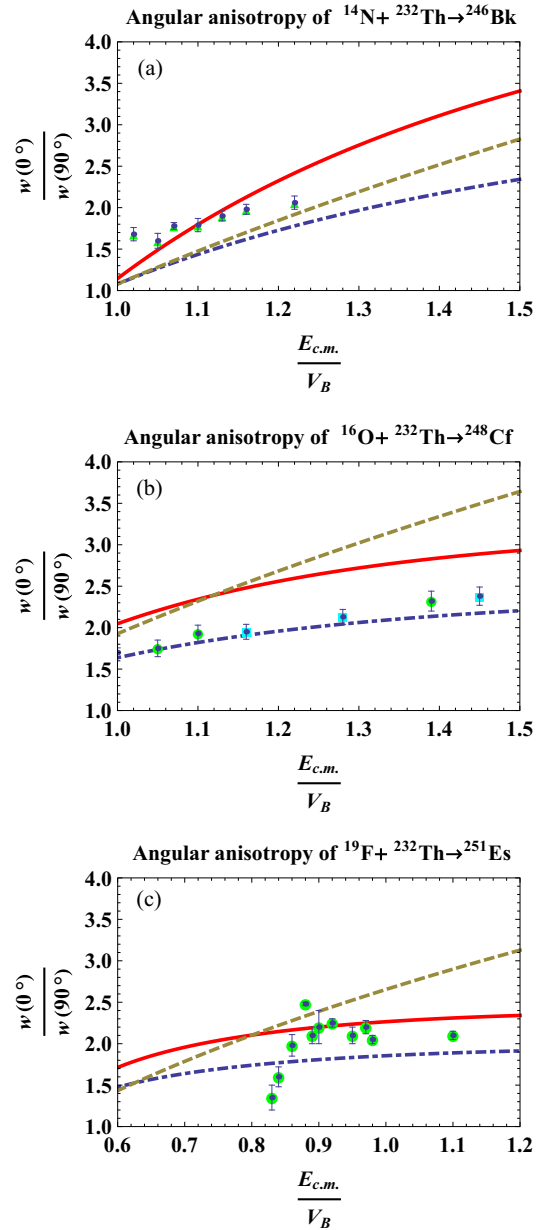


FIG. 3. (Color online) Experimental fission fragment angular distributions for the induced fission of the ^{232}Th by different projectiles are compared with the predictions of the SSPS (dot-dashed curve), the SPS (dashed curve), and the USPS (continuous curve). (a) For the induced fission of the ^{232}Th target by ^{14}N , the experimental values of angular anisotropy denoted by triangles are taken from Ref. [28]. (b) For the induced fission of the ^{232}Th target by ^{16}O , the experimental values of angular anisotropy denoted by circles and squares are taken from Refs. [17,29], respectively. (c) For the induced fission of the ^{232}Th target by ^{19}F , the experimental values of angular anisotropy denoted by circles are taken from Ref. [32].

reaction dynamics. The Businaro-Gallone mass asymmetry parameter α_{BG} is parametrized as $\alpha_{\text{BG}} = 0$ for $\chi < \chi_{\text{BG}}$, and $\alpha_{\text{BG}} = 1.12 \sqrt{\frac{(\chi - \chi_{\text{BG}})}{(\chi - \chi_{\text{BG}}) + 0.24}}$ for $\chi > \chi_{\text{BG}}$, where χ is the fissility parameter, and $\chi_{\text{BG}} = 0.396$ [33,34]. For the systems having

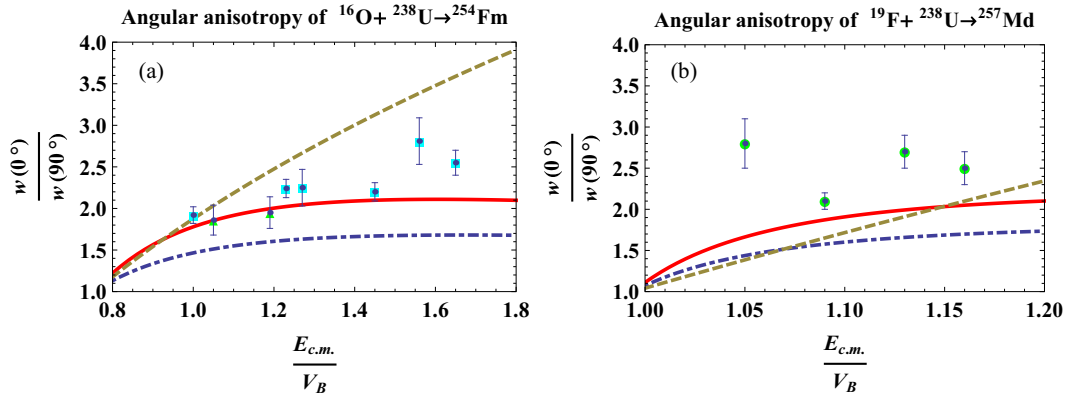


FIG. 4. (Color online) Experimental fission fragment angular distributions for the induced fission of the ^{238}U by different projectiles are compared with the predictions of the SSPS (dot-dashed curve), the SPS (dashed curve), and the USPS (continuous curve). (a) For the induced fission of the ^{238}U target by ^{16}O , the experimental values of angular anisotropy denoted by squares and triangles are taken from Refs. [17,30], respectively. (b) For the induced fission of the ^{238}U target by ^{19}F , the experimental values of angular anisotropy denoted by circles are taken from Ref. [31].

the entrance channel mass asymmetry parameter α larger than the Bussinaro-Gallone mass asymmetry α_{BG} , values of anisotropies are normal, while for systems having α smaller than α_{BG} , the measured anisotropy values are much larger than the SSPS model predictions. Table III includes the entrance channel mass asymmetry parameter α , Businaro-Gallone mass asymmetry parameter α_{BG} , and $n(\alpha)$ for the systems. The entrance channel mass asymmetry parameter for the all studied systems is smaller than the Businaro-Gallone mass asymmetry parameter as shown in Table III. The USPS model is also tested for the two $^{32}\text{S} + ^{197}\text{Au}$ and $^{16}\text{O} + ^{248}\text{Cm}$ reaction systems. Figure 5 is shown the calculated angular anisotropies based upon the SSPS, the SPS, and the USPS models for the two reaction systems. It is observed that the fission fragment angular distributions calculated based upon the USPS model are able to explain consistently the energy dependence of the angular anisotropies for the two systems.

V. SUMMARY AND CONCLUSIONS

Fission fragment angular distributions for the eight reaction systems with an anomalous behavior within the framework of the standard saddle-point statistical, the scission-point statistical, and the upgraded saddle-point statistical are calculated. The prediction of the upgraded saddle-point statistical model for the studied systems are found in better agreement with the experimental data of angular anisotropies than the predictions of the standard saddle-point statistical and the scission-point statistical models. In addition, the upgraded saddle-point statistical model is tested for the two reaction systems with an anomalous behavior anisotropy. It is observed that the upgraded saddle-point statistical model also acts more successful for these two systems than the two other models. As a result, the upgraded saddle-point statistical model can be used to predict the anomalous angular fragment distributions for most reaction systems with anomalous fragment anisotropies.

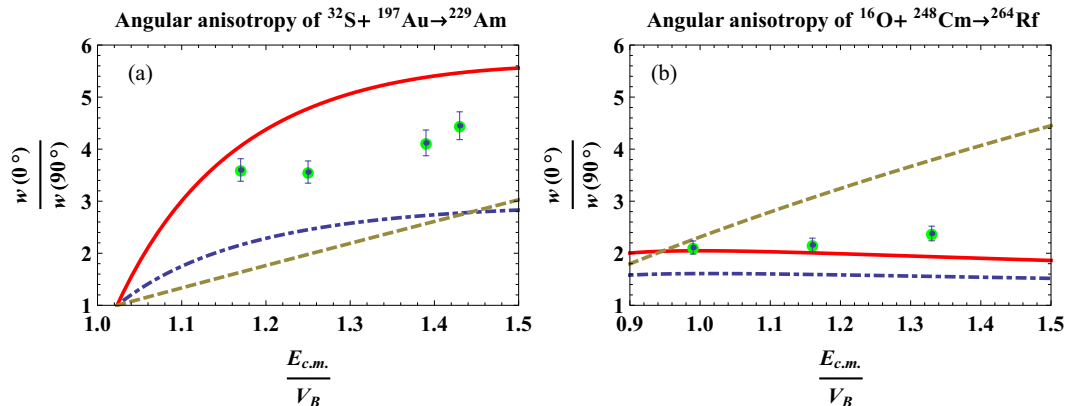


FIG. 5. (Color online) Experimental fission fragment angular distributions for the induced fission of the $^{32}\text{S} + ^{197}\text{Au}$ and $^{16}\text{O} + ^{248}\text{Cm}$ reaction systems are compared with the predictions of the SSPS (dot-dashed curve), the SPS (dashed curve), and the USPS (continuous curve). (a) For the induced fission of $^{32}\text{S} + ^{197}\text{Au}$, the experimental values of angular anisotropy denoted by circles are taken from Ref. [17]. (b) For the induced fission of $^{16}\text{O} + ^{248}\text{Cm}$, the experimental values of angular anisotropy denoted by circles are taken from Ref. [17].

TABLE III. The entrance channel mass asymmetry parameter, Businaro-Gallone mass asymmetry parameter, and $n(\alpha)$ for the studied reaction systems.

Heavy-ion-induced fission system	α	α_{BG}	$n(\alpha)$
$^{24}\text{Mg} + ^{208}\text{Pb}$	0.793	0.877	0.815
$^{28}\text{Si} + ^{208}\text{Pb}$	0.763	0.894	0.758
$^{32}\text{S} + ^{208}\text{Pb}$	0.733	0.901	0.662
$^{14}\text{N} + ^{232}\text{Th}$	0.866	0.894	0.737
$^{16}\text{O} + ^{232}\text{Th}$	0.871	0.897	0.776
$^{19}\text{F} + ^{232}\text{Th}$	0.849	0.900	0.815
$^{16}\text{O} + ^{238}\text{U}$	0.874	0.903	0.769
$^{19}\text{F} + ^{238}\text{U}$	0.852	0.905	0.810

- [1] R. Vandenbosch and J. R. Huizenga, *Nuclear Fission* (Academic Press, New York, 1973).
- [2] H. H. Rossner, J. R. Huizenga, and W. U. Schröder, *Phys. Rev. Lett.* **53**, 38 (1984).
- [3] S. Kailas, *Phys. Rep.* **284**, 381 (1997).
- [4] L. C. Vaz and J. M. Alexander, *Phys. Rep.* **97**, 1 (1983).
- [5] P. D. Bond, *Phys. Rev. Lett.* **52**, 414 (1984).
- [6] P. D. Bond, *Phys. Rev. C* **32**, 471 (1985).
- [7] S. Soheyli and M. K. Khalili, *Phys. Rev. C* **85**, 034610 (2012).
- [8] J. P. Lestone, A. A. Sonzogni, M. P. Kelly, and R. Vandenbosch, *Phys. Rev. C* **56**, R2907(R) (1997).
- [9] J. C. Mein, D. J. Hinde, M. Dasgupta, J. R. Leigh, J. O. Newton, and H. Timmers, *Phys. Rev. C* **55**, R995 (1997).
- [10] W. J. Swiatecki, *Phys. Scr.* **24**, 113 (1981).
- [11] S. Bjornholm and W. J. Swiatecki, *Nucl. Phys. A* **391**, 471 (1982).
- [12] J. P. Blocki *et al.*, *Nucl. Phys. A* **459**, 145 (1986).
- [13] C. Ngo, *Prog. Part. Nucl. Phys.* **16**, 139 (1986).
- [14] C. Lebrun, F. Hanappe, J. F. LeColley, F. Lefebvres, C. Ngo, J. Peter, and B. Tamain, *Nucl. Phys. A* **321**, 207 (1979).
- [15] V. S. Ramamurthy and S. S. Kapoor, *Phys. Rev. Lett.* **54**, 178 (1985).
- [16] V. S. Ramamurthy *et al.*, *Phys. Rev. Lett.* **65**, 25 (1990).
- [17] B. B. Back *et al.*, *Phys. Rev. C* **32**, 195 (1985).
- [18] D. Vorkapic and B. Ivanisevic, *Phys. Rev. C* **52**, 1980 (1995).
- [19] D. J. Hinde, M. Dasgupta, J. R. Leigh, J. P. Lestone, J. C. Mein, C. R. Morton, J. O. Newton, and H. Timmers, *Phys. Rev. Lett.* **74**, 1295 (1995).
- [20] A. Saxena, S. Kailas, A. Karnik, and S. S. Kapoor, *Phys. Rev. C* **47**, 403 (1993).
- [21] R. D. Butt, D. J. Hinde, M. Dasgupta, A. C. Berriman, A. Mukherjee, C. R. Morton, and J. O. Newton, *Phys. Rev. C* **66**, 044601 (2002).
- [22] Zuhua Liu, Huanqiao Zhang, Jincheng Xu, Yu Qiao, Xing Qian, and Chengjian Lin, *Phys. Rev. C* **54**, 761 (1996).
- [23] H. Halpern and V. M. Strutinski, in *Proceedings of the Second United Nations International Conference on the Peaceful Uses of Atomic Energy, Geneva, Switzerland, 1955* (United Nations, Geneva, Switzerland, 1958), p. 408.
- [24] H. Rossner, J. R. Huizenga, and W. U. Schröder, *Phys. Rev. C* **33**, 560 (1986).
- [25] S. Cohen, F. Plasil, and W. J. Swiatecki, *Ann. Phys. (NY)* **82**, 557 (1974).
- [26] A. J. Sierk, *Phys. Rev. C* **33**, 2039 (1986).
- [27] B. B. Back, R. R. Betts, K. Cassidy, B. G. Glagola, J. E. Gindler, L. E. Glendenin, and B. D. Wilkins, *Phys. Rev. Lett.* **50**, 818 (1983).
- [28] B. R. Behera, M. Satpathy, S. Jena, S. Kailas, R. G. Thomas, K. Mahata, A. Chatterjee, S. Roy, P. Basu, M. K. Sharan, and S. K. Datta, *Phys. Rev. C* **69**, 064603 (2004).
- [29] S. Kailas, D. M. Nadkarni, A. Chatterjee, A. Saxena, S. S. Kapoor, R. Vandenbosch, J. P. Lestone, J. F. Liang, D. J. Prindle, A. A. Sonzogni, and J. D. Bierman, *Phys. Rev. C* **59**, 2580 (1999).
- [30] W. Q. Shen *et al.*, *Phys. Rev. C* **36**, 115 (1987).
- [31] A. Karnik, S. Kailas, A. Chatterjee, A. Navin, A. Shrivastava, P. Singh, and M. S. Samant, *Phys. Rev. C* **52**, 3189 (1995).
- [32] N. Majumdar, P. Bhattacharya, D. C. Biswas, R. K. Choudhury, D. M. Nadkarni, and A. Saxena, *Phys. Rev. Lett.* **77**, 5027 (1996).
- [33] U. L. Businaro and S. Gallone, *Il Nuovo Cimento* **5**, 315 (1957).
- [34] M. Abe, KEK Report No. 86-26, KEK TH-28, 1986.